

# The effect of clay water content in the Jet Erosion Test

Raniero Beber<sup>1,\*</sup>, Alessandro Tarantino<sup>1</sup>, Matteo Pedrotti<sup>1</sup>, and Rebecca Lunn<sup>1</sup>

<sup>1</sup>University of Strathclyde, Department of Civil and Environmental Engineering, Glasgow, UK

**Abstract.** The understanding of the onset of breaching induced by surface erosion is fundamental to enable definition of the level of protection afforded by embankments and provision of standards for the design of new structures and the upgrading of existing ones. Compacted embankment materials are generally partially saturated due to seasonal variation in the water content. At the onset of the overflow process embankments undergo to a wetting process due to the changes at the outer surface boundary conditions (i.e. overflow). Erosion behaviour is known to be a counterbalance between gravity forces and shear erosion forces. However, as the particle size decreases (i.e. clayey soils), gravitational forces become negligible and electrochemical interaction between particles play a dominant role. Clay microstructure (e.g. particle configuration and inter-particle forces) changes with the hydro-mechanical stresses history. Thus, it is necessary to consider the microstructural changes in particle configuration to understand the influence of microstructure on the macroscopic behaviour of clay during erosion. Upon wetting, clay have a swelling/collapse behaviour. This research presents experimental results on erosion of clay samples compacted at the same initial dry density but with different compaction water content. The influence of different wetting times on erosion is also investigated. We show that for a given as-compacted water content, the longer the wetting stage, and hence the higher the sample water content, the more erodible the samples. Additionally, for samples compacted at the same dry density, the ones compacted on the dry side of optimum are more erodible than samples compacted at the optimum water content, despite the lower water content at formation. We hypothesise that this may be due to the formation of a different initial microstructure in sample on the dry side of optimum (i.e. bi-modal pore size distribution). Our results contribute to the fundamental understanding of time-dependent mechanisms that influence erosion of clay embankments during overflow and, hence, to embankment failure. In addition, these tests show how basic concepts of unsaturated soil mechanics can serve as a guide to ‘design’ the compaction conditions of embankment material.

## 1 Introduction

A recent review of 76 reservoir incidents that occurred in the UK in the period 2004-2013 highlights that erosion by flood overtopping is the main mechanism of embankment deterioration [1]. The Environment Agency in the National Strategy of 2011 [2] estimates that UK has 9000 km of linear raised flood defences, which mainly consist of soil embankments. Simm et al. [3], reviewed the impact of five major flood events on these structures during the period 2007-2016 with the conclusion that English levees were rarely breached, and that when breaching did occur, the dominant failure mechanism was overflow and rear face erosion, which are then impacted further by local irregularities. These earthen structures are historic, with an average age of 125 years, the oldest structure being 800 years. Their age introduces uncertainty as to the real status of the English flood defence infrastructure network when subject both to seasonal and extreme loading events. To reduce this uncertainty, a fundamental understanding of the onset of breaching-induced surface erosion is required so as to better define the levels of protection afforded by his-

toric embankments, to provide standards for the design of new structures and to derive strategies for upgrading of existing ones.

Erosion behaviour is known to be a counterbalance between gravity forces and shear erosion forces [4]. However, as the particle size decreases, as in clayey soils, gravitational forces become negligible and electrochemical interaction between particles dominates. Clay microstructure (particle configuration and inter-particle forces) changes with the hydro-mechanical stress history [5, 6]. Upon wetting, clay manifests a swelling/collapse behaviour. It is necessary, therefore, to consider fundamental changes to the microstructural particle configuration in order to understand the influence of microstructure on the macroscopic behaviour of clay during erosion.

Almost all earthen structures are built by compacting clayey soils to improve their mechanical properties; hence, it is important to understand the load posed by flood water. Compacted embankment soils are generally partially saturated due to the seasonal variation in water content. At the onset of an overflow process, embankments undergo wetting due to the change of conditions at the outer surface boundary conditions.

\*e-mail: [raniero.beber@strath.ac.uk](mailto:raniero.beber@strath.ac.uk)

In the literature, due to a historical dominance of loose boundary hydraulics research, particular effort has been spent in characterizing the hydraulic load applied to a sample by a water impinging jet (i.e. the pressure fields and the stress distribution on the impinged surface [4, 7, 8]). However, since erosion processes are not only controlled by erosive forces (applied water shear stress) but also by resisting forces such as particle interactions, it appears there is a fundamental need to characterize soil properties, and their evolution, in the same detail.

To date, little attention has been paid to the effect of the soil hydro-mechanical conditions on erosion.

In this study, the role of clay microstructure on erosion mechanisms and scour evolution in kaolin clay is investigated under varying conditions of compaction water content and wetting time. The Jet Erosion Test (JET) [7] was chosen since it is commonly applied and the exposed surface of the sample allows a direct comparison with the wetting process that occurs in the field.

## 2 Material and Specimen Preparation

The clay chosen for the tests presented here is Speswhite™ Kaolin from Imerys with a plastic limit  $\omega_{PL} = 0.32$  and a liquid limit  $\omega_{LL} = 0.64$ . The particle size distribution has a 0.20 silt fraction and a 0.80 clay fraction.

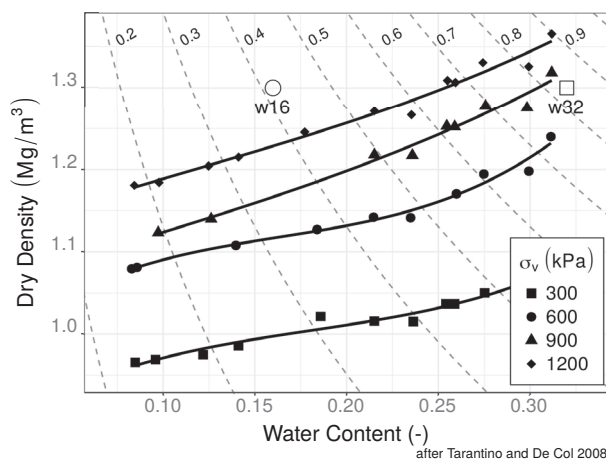


**Fig. 1.** Compaction curves for kaolin clay at different vertical stresses [9]. The iso-saturation curves are drawn in grey dashed lines while the as-compacted conditions of the samples ‘w16’ and ‘w32’ are marked for gravimetric water content of 0.16 and 0.32 respectively.

Specimen preparation consisted of two stages: 1) compaction of the specimen; 2) wetting of the compacted specimen. Here a distinction between the water contents of the specimens at the two stages is needed: the ‘at compaction’ water content refers to the original formation water influencing the initial microstructure; whereas the water content ‘post wetting’ refers to the degree of saturation of the specimen prior to initiation of the JET test.

Samples were compacted at two different water contents (0.16 and 0.32), with the same dry density (1.3 Mg/cm<sup>3</sup>). In Figure 1 the dry density and water content of the two compacted samples (defined as ‘w16’ and

‘w32’) are compared with the compaction plane from [9] where the same material was used. For each target water content, the specimens were compacted in acrylic cylindrical moulds of 100 mm in height, an internal diameter of 100 mm and a wall thickness of 5 mm.

Three specimens were compacted (*stage 1*) with the dry density and water content for sample ‘w16’ in Figure 1 and a further two samples for ‘w32’. In order to reach the two target water contents, oven dry kaolin powder was moisturized with distilled water in thin layers in a plastic batch, mixed with sharp spatulas and let homogenize in sealed plastic bags for 24 hours, as described in [10]. After moisture equalization the material was sieved with Woven wire 1 mm mesh sieve, the water content of the sieved material was checked against the target.

Static compaction was achieved using displacement control equipment, the specified dry density was achieved and the force required to reach the target volume was recorded. This process was performed in one single layer to avoid any stratification that could affect the dynamics of the subsequent wetting process. Compacted samples were stored in sealed bags for 24 hours before testing.

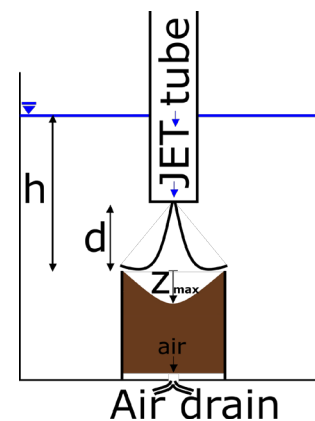


**Fig. 2.** Schematic of the JET erosion test apparatus utilized in this study. The air drain is added to the original design [7] to allow the expel of air pushed by the advancing wetting front.

The wetting (*stage 2*) of the specimens was performed in the JET apparatus (prior to JET testing), within which a 200 mm head above the top of the mould ( $h$  in Figure 2) was applied to the top of the sample, whilst the bottom end was connected to an air drain to inhibit air-pressure build up due to the advancing wetting front.

Three different wetting times were chosen for sample ‘w16’: specimen ‘w16-1’ was submerged for 1 hour before the JET test, specimen ‘w16-3’ for 3 hours, and specimen ‘w16-6.5’ for 6.5 hours. For sample ‘w32’ specimen ‘w32-1’ was submerged for 1 hour and specimen ‘w32-6.5’ for 6.5 hours.

## 3 Experimental Procedure

The specimens were tested within the JET apparatus described in [7], a schematic of which is reported in Figure 2. During the JET test, sample erosion is caused by a submerged impinging water jet normal to the surface of the

sample. The jet is generated by a 6.4 mm nozzle obstructing the constant head flow from a tank. The sample holder container at the bottom provides the output constant head ( $h$  in Figure 2) and a constant bearing pressure to the specimen. After a given wetting time, each specimen is tested under the same JET conditions: a 1240 mm driving water head for the jet applied for 5 minutes with the nozzle 40 mm from the surface of the mould ( $d$  in Figure 2). The distance  $d$  between the top surface of the mould and the JET nozzle is conventionally kept constant in the literature between each series of tests. The one adopted in this study is 40 mm. The static water head above the mould ( $h$  in Figure 2), was kept constant during each testing and equal to the 200 mm used during the wetting stage.

The surface of the sample before and after the erosion test was recorded using a scanCONTROL 2700-100/BL laser scanner from Micro-Epsilon. The point cloud difference between pre and post erosion scans allows for computation of the eroded volume and the maximum scour depth.

### 4 Experimental Observations

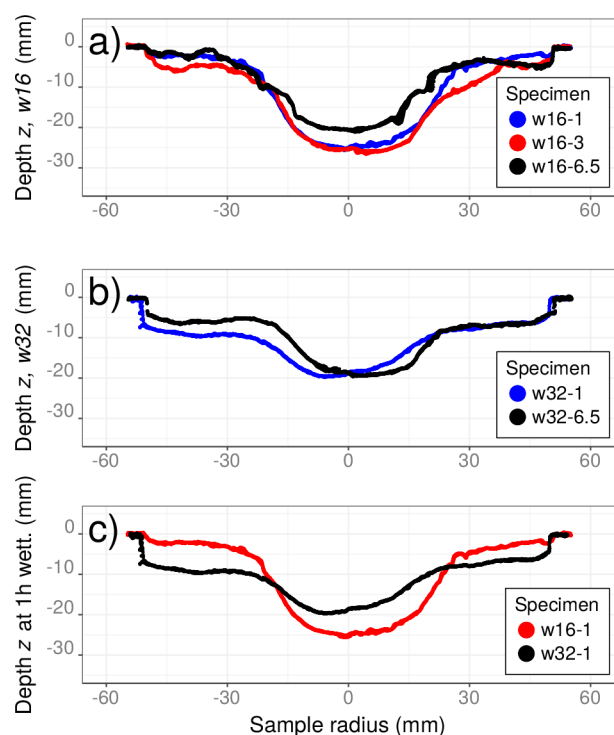


**Fig. 3.** Scour profile sections from point clouds obtained via the laser scanner. a) The final scour shape for three different wetting times for samples with an as-compacted water content of 0.16, 'w16' and b) final scour shape for two different wetting times for samples with an as-compacted water content of 0.32, 'w32'; c) comparison between the two scour profiles for 1 hour of wetting with different as-compacted water contents i.e. specimens 'w16-1' and 'w32-1'.

Figure 3a reports the final scour profiles with increasing specimen wetting time for sample with an as-compacted water content of 0.16. In Figure 3a, the scour profile deepens slightly from specimen 'w16-1' to specimen 'w16-3' as the pre-test wetting time increases from 1

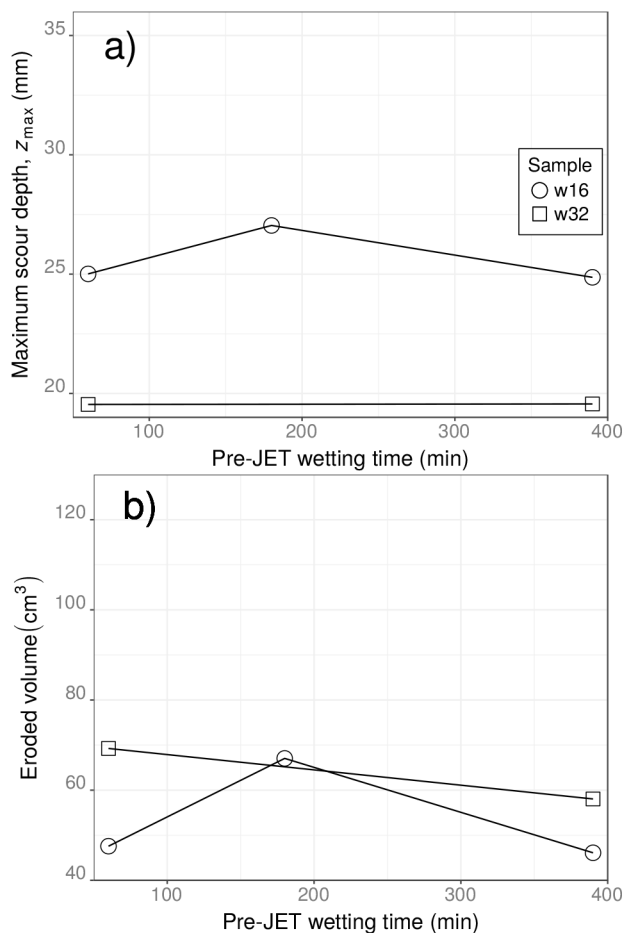


**Fig. 4.** Erosion dependency on wetting time. a) maximum depth of scour close to the centre of the sample, b) total eroded volume. Measurements relative to the post compaction state of the specimen.

to 3 hours. The greatest difference is found for specimen 'w16-6.5' for which both the areal extent and the depth of the scour profile are significantly smaller than those with either 1 or 3 hours of wetting.

In Figure 3b samples 'w32', with an as-compacted water content of 0.32, show a bell shape scour for both of the submergence times. At 6.5 hours the scour of the specimen 'w32-6.5', as with sample 'w16', is less deep and slightly smaller than for specimen 'w32-1'.

For comparison, the scour of specimens 'w16-1' and 'w32-1' with a wetting time of 1 hour are reported in Figure 3c. Clear from the Figure is that 'w16-1' has a deeper profile with a narrower diameter, whereas 'w32-1' has a relatively shallow erosion profile with evidence of significant material loss across the full surface.

Figure 4 reports the maximum scour depth and the eroded volume calculated as the point cloud difference between the as compacted specimen (before wetting) and the post JET scoured specimen.

In Figure 4a the influence of pre-JET wetting time to the maximum scour depth,  $z_{max}$  is illustrated. It appears that the wetting time does not have a major effect on the scour depth of the samples. The initial as compacted water content of the samples, however, does have a significant

effect, with the lower water content consistently resulting in a narrower and deeper scour profile.

Figure 4b shows results from the same experiments as those plotted in Figure 4a, but for the eroded soil volume, calculated as the point cloud difference between the as compacted specimen (before wetting) and the post JET scoured specimen. The eroded soil volume appears to decrease with an increase in the duration of the wetting time and the relationship to the as compacted water content is slightly unclear, these latter results might be explained by looking at the cross sections in Figure 3c, in which the wider scours have a bigger contributing area, thus more volume is eroded. For two out of three samples, the eroded soil volume is greater for the sample with the higher as-compacted water content. The data herein report results from single specimens. Thus, the increase at 3h of total eroded volume observed in Figure 4b may be due to experimental error.

According to [4] the distribution of shear stress applied by the water jet depends on the shape of the scour close to the centre line of the jet. Therefore, the only section where an actual comparison between different samples is possible for the JET test is the central part of the sample where the shear stresses are at a maximum. The data plotted in Figure 4b, where the eroded volume is calculated, use the entire sample cross-sectional area. Consequently, these data are not processed any further, as it is believed that the different samples are not directly comparable, because applied shear stresses in the area off the centre line of the sample will differ. Hence, in the remaining of the paper we refer only to the depth of scour.

Figures 3a,b and 4a show that as the wetting time increases from 1 to 3 to 6.5 hours there is very little change in the erodibility of the samples. These results are counterintuitive, since as the water content increases, the suction within the sample is expected to decrease and thus the provided apparent cohesion at ‘quasi-zero’ vertical stress [10]. Hence, samples with a high water content should be more erodible.

This behaviour might be explained if the change in density that occurs during the wetting stage is taken into account.

## 5 Considering wetting

The wetting process in the JET was monitored via photography and the height of swelling was determined by processing images at the start and end of the wetting phase. Figure 5 shows the swelling height estimated at 1, 3 and 6.5 hours of wetting before initiation of the JET. As expected, the sample swelling increases (thus density reduced) as the duration of the wetting phase increases. Samples ‘w32’ swell more than samples ‘w16’.

To take account of the swelling of the sample, and hence the change in elevation of the sample surface, the maximum scour depth was corrected using equation 1, where,  $z^*$  is the corrected scour depth,  $\Delta z$  is the swelling height at the start of the JET test and  $z_{max}$ , is the measured

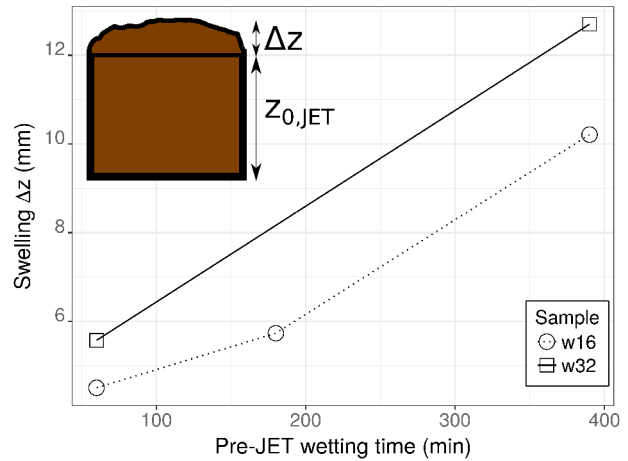


**Fig. 5.** Free swelling upon wetting estimated from image processing for samples ‘w16’ and ‘w32’ tested in the JET at different wetting time.

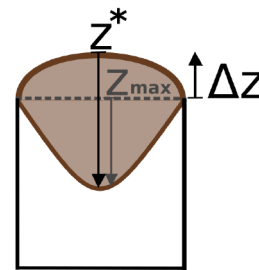


**Fig. 6.** Schematic representing the correction described in equation 1. The JET raw  $z_{max}$  is corrected considering the swelling  $\Delta z$  induced by the wetting process.

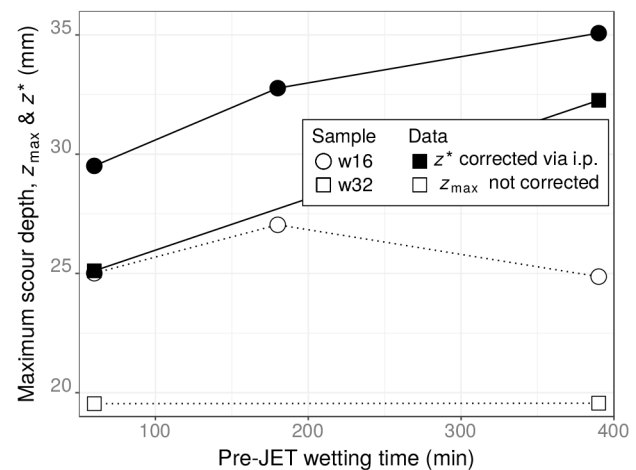


**Fig. 7.** Corrected erosion dependency of maximum depth of scour close to the centre of the sample on wetting time. The corrected dataset is essentially the sum of data from Figure 4a and 5 as in equation 1.

scour depth (Figure 6).

$$z^* = z_{max} + \Delta z \quad (1)$$

In Figure 7 the corrected scour depth,  $z^*$ , for all samples is plotted, alongside the original scour depth,  $z_{max}$ , from Figure 4a. Figure 7 shows that for both the ‘w16’ and the ‘w32’ samples, the corrected scour depth increases as the wetting time increases. Thus, the samples do in-

deed become more erodible as the degree of saturation, prior to JET test initiation, increases. Considering the at compaction water content, sample 'w32' which has a water content near optimum (see Figure 1) is more resistant to erosion than sample 'w16'.

## 6 Effects of the 'at-compaction' microstructure on wetting

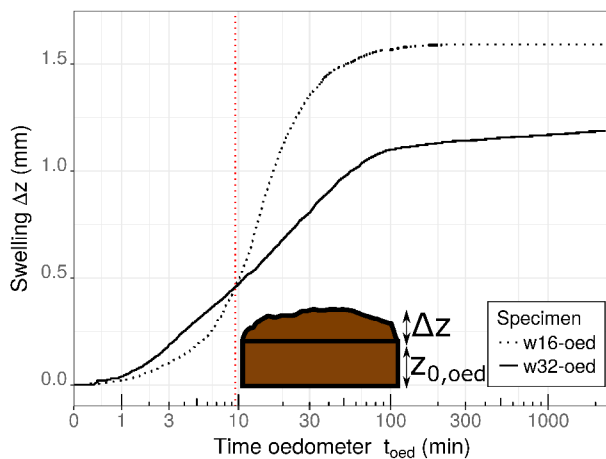


**Fig. 8.** Free swelling curves upon wetting obtained in oedometer for specimen 'w16-oed' and 'w32-oed' compacted at the same condition as the one tested in the JET of Figure 1.

The data presented in Figure 7 suggest that the samples formed at higher water content ('w32'), and therefore at lower initial suction, are less erodible than the samples prepared at lower water content ('w16'), where the suction at formation is higher. This is perhaps not as expected, since the higher suction should increase the provided apparent cohesion at 'quasi-zero' vertical stress.

Figure 5 shows the swelling for all samples, as measured prior to the JET test. In order to better understand the swelling behaviour of the different as-compacted water contents, equivalent free swelling curves were measured in the oedometer. Two specimens, 'w16-oed' and 'w32-oed', were compacted in a standard oedometer cell at water contents equal to 0.16 and 0.32 respectively, with the same dry density as the samples used in the JET. The wetting of these samples compacted in the oedometer cell was monitored in continuous mode following the entire evolution using a potentiometer displacement transducer. In the oedometer, samples were wetted from the bottom porous stone using the same constant head that was provided for the wetting in the JET apparatus, of 20 mm above the surface of the as compacted sample which in the oedometer had a thickness of 10 mm.

Figure 8 shows the free swelling curves obtained in the oedometer. At early time, up to 9.5 minutes, the swelling is higher for specimen 'w32-oed' (the red line in Figure 8) than for 'w16-oed'. However, the final swelling is greater for specimen 'w16-oed'. The end of swelling can be estimated by the Casagrande method [11] locating the  $t_{90}$  at approximately 30 min and 70 min for specimens 'w32-oed' and 'w16-oed' respectively.

Sample 'w16', is compacted on the dry side of optimum (see Figure 1), hence, prior research (amongst the many [5, 12–14], and more recently [6]) shows that the microstructure presents a double porosity. Sample 'w32', is near the optimum, and thus presents a single porosity. According to Pedrotti [6], in compacted specimens, upon wetting micropores swell and macropores collapse. The ratio between the two mechanisms controls whether the specimens collapse or swell. Accordingly, under unconfined conditions, the two samples ('w16 and 'w32') swell with different rates and magnitudes.

Macropores have a higher hydraulic conductivity than the micropores and, therefore, collapse is expected to dominate in the initial stages of the wetting for specimen 'w16-oed'. This explains the gradually increasing rate of swelling in sample 'w16-oed' (Figure 8).

Figure 8 shows that, for the first 9.5 minutes, specimen 'w32-oed' swells faster than specimen 'w16-oed' after which the situation is reversed. This suggests that the larger volume samples tested in the JET are still in the initial wetting phase, as Figure 5 shows that 'w16' swell less than 'w32'.

Assuming that the samples are formed in the same conditions and have the same consolidation coefficient  $C_v$ , the swelling time in the JET can be normalized and compared with the swelling time in the oedometer.

From equation 2, where the non-dimensional times of the swelling are equal, it is possible to derive equation 3 for the scaling time,  $t^*$  where subscripts  $JET$  and  $oed$  refer to the JET and the oedometer respectively,  $t$  is the elapsed time in the wetting process and  $z_0$  is the respective drainage height.

$$\frac{C_v t_{JET}}{z_{0,JET}^2} = \frac{C_v t_{oed}}{z_{0,oed}^2} \quad (2)$$

$$t^* = t_{oed} = \frac{z_{0,oed}^2}{z_{0,JET}^2} t_{JET} \quad (3)$$

In Figure 9, the comparison of the two swelling datasets shows that, as already speculated, the wetting of the samples in the JET test was still in the initial phase.

The difference in swelling magnitude shown on Figure 9 between the sample in the acrylic mould (JET) and the samples in the oedometer is likely due to the drain path in the oedometer cell (10mm) being much smaller than in the acrylic mould (100mm).

## 7 Effects of the 'at-compaction' microstructure on erosion

The corrected data in Figure 7 show the samples with an as-compacted moisture content of 0.16 to be consistently more erodible than those of 0.32. As previously observed this is counterintuitive, as the suction in the sample with the lower as-compacted moisture content should be higher. Thus providing a higher apparent cohesion. One explanation for the sample 'w16' being more erodible may be the microstructure formed during compaction. As the sample 'w16' is on the dry side of optimum, it was shown to

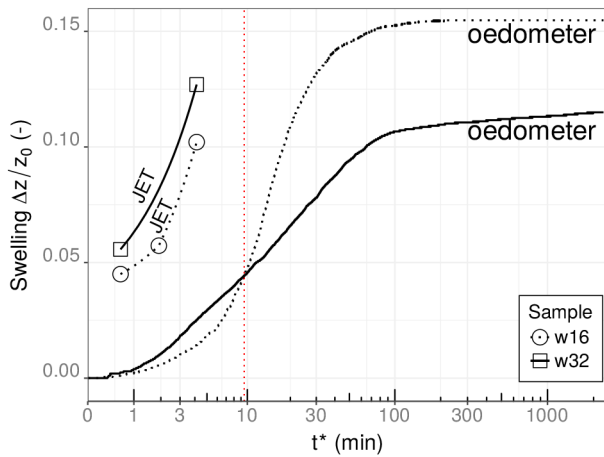


**Fig. 9.** Comparison between free swelling curves upon wetting obtained in oedometer and in the JET mould for samples ‘w16’ and ‘w32’ compacted at the same conditions (see Figure 1). The time of the JET curves has been scaled with equation 3 and the swelling normalized by the height of the compacted samples.

have a bi-modal pore size distribution (i.e. two dominant classes of pores are present: macropore and micropores), whereas the sample ‘w32’ presents a mono-modal pore size distribution (i.e. the micropores class is the dominant class of pores). The presence of macropores in sample ‘w16’ will locally increase the hydraulic conductivity of the sample and facilitate the removal of groups of particles. This phenomenon may accelerate the erosion process.

## 8 Conclusion

In this study the role of clay microstructure on erosion mechanisms and scour evolution in kaolin clay was investigated in terms of the effects of compaction water content and the water content prior to erosion testing. It has been shown that both the formation water content of the compacted clay and the initial wetting time effect the erosion rate. In order to interpret JET erosion tests with material such as clay that are prone to swelling test results must be corrected by considering the change to sample height caused by the ongoing swelling during the test. Erosion test results show that:

- For a given as-compacted water content, the longer the wetting stage, and hence the higher the sample water content, the more erodible the samples.
- For samples compacted at the same dry density, the ones compacted on the dry side of optimum are more erodible than samples compacted at the optimum water content, despite the lower water content at formation. We hypothesise that this may be due to the formation of a different initial microstructure in sample on the dry side of optimum (i.e. bi-modal pore size distribution), and thus causing a different erosion mechanism.

Our results contribute to the fundamental understanding of time-dependent mechanisms that influence erosion of clay embankments during overflow and, hence, to embankment failure. In addition, these tests show how basic concepts of

unsaturated soil mechanics can serve as a guide to ‘design’ the compaction conditions of embankment material.

The authors wish to acknowledge the support of the European Commission via the Marie Skłodowska-Curie Innovative Training Networks (ITN-ETN) project TERRE ‘Training Engineers and Researchers to Rethink geotechnical Engineering for a low carbon future’ under grant agreement ETN-GA-2015-675762.

## References

- [1] C. Mitchell, O. Tarrant, T. Deakin, *An overview of levees and reservoirs in England*, in *3rd Inter. Conf. on Protection against Overtopping* (2018)
- [2] EA, *Understanding the risks, empowering communities, building resilience: the national flood and coastal erosion risk management strategy for England* (DEFRA, 2011)
- [3] J. Simm, J. Flikweert, C. Hollingsworth, O. Tarrant, *Ten years of lessons learned from English levee performance during severe flood events*, in *85th Annual Meeting of Inter. Comm. on Large Dams. ICOLD* (2017)
- [4] F. Mercier, F. Golay, S. Bonelli, F. Anselmet, R. Borghi, P. Philippe, *European Journal of Mechanics-B/Fluids* **45** (2014)
- [5] A. Tarantino, *Unsaturated soils*. Edited by EE Alonso and A. Gens. CRC Press (2011)
- [6] M. Pedrotti, A. Tarantino, *Géotechnique* **69** (2019)
- [7] G. Hanson, K. Cook, *Applied Eng. in Agri.* **20** (2004)
- [8] S.M. Ghaneeizad, J.F. Atkinson, S.J. Bennett, *Env. Fluid Mechanics* **15** (2015)
- [9] A. Tarantino, E. De Col, *Géotechnique* **58** (2008)
- [10] A. Tarantino, S. Tombolato, *Géotechnique* **55** (2005)
- [11] A. Casagrande, R. Fadum, *Notes on soil testing for engineering purposes* (Graduate School of Engineering, Harvard University, 1940)
- [12] E. Romero, G. Della Vecchia, C. Jommi, *Géotechnique* **61** (2011)
- [13] R. Monroy, L. Zdravkovic, A. Ridley, *Géotechnique* **60** (2010)
- [14] M. Pedrotti, A. Tarantino, *Géotechnique* **68** (2018)